

A posteriori modeling error estimates in the optimization of two-scale elastic composite materials

Sergio Conti^{*} Benedict Gei[†] Martin Lenz[†] Martin Rumpf[†]

November 16, 2015

Abstract

The design of optimal composite elastic materials within a two-scale linearized elasticity model is studied in this paper. We consider a mechanically simple, constructible parametrized microscopic supporting structure, whose parameters are determined minimizing the compliance objective. Nested laminates are known to realize the minimal compliance and provide a benchmark for the quality of the microstructures. Our microstructures achieve the optimal value of the compliance up to a few percent. We further estimate the origin of this mismatch, and in particular the local difference in the compliance functional between simulations with simple parametrized structures and the ones with optimal nested laminates. To this end a dual weighted residual approach is applied to derive a posteriori error indicators for the compliance functional tracking both the numerical error due to the discretization and the modeling error of the approximating two-scale composite material. Different numerical experiments show that the resulting adaptive scheme leads to simple parametrized microscopic supporting structures that can compete with the optimal nested laminate construction. In particular, our error indicators show how discretization error and modeling error can be balanced by choosing an optimal level of grid refinement.

1 Introduction

It is a fundamental insight in shape optimization that elastic bodies subjected to external surface loadings exhibit the spontaneous development of microstructures, for example in the case of compliance optimization [3]. This phenomenon is a practical manifestation of the fact that the associated minimization problem is in general ill-posed. One popular solution appeals to relaxation theory, thereby allowing composite materials with intermediate density and effective elasticity tensors resulting from a microscopic mixture of the involved constituents. Homogenization theory [20, 44] is then used to derive the effective material properties of a composite elastic material, starting from a given microscopic decomposition into homogeneous regions of the individual ingredient materials. Using the G-closure theory [18, 44] it can be shown that a nested lamination structure realizes the minimal value of the compliance functional [3]. Let us note that optimal constructions exist but are not unique. In fact, several entirely different microstructures lead to globally optimal material properties at the macroscopic level [18, 44]. Most of them are however purely theoretical, lack a truly mechanical equivalent and would not be manufacturable. We address this optimal design problem for 2D elastic material composites numerically and introduce a microscopic supporting structure consisting of two orthogonal trusses with varying thickness and arbitrary rotation (cf. Figure 1). For these simple microscopic cell geometries a collocation type boundary element method is employed to compute the corrector problem in a two-scale ansatz and to evaluate the local effective elasticity tensor. This is then combined with a bi-quadratic finite element scheme on a rectangular grid on the macroscale to set up a two-scale approach for the simulation of microstructured composite elastic materials. We shall in particular focus on a microscopic construction with rotated, orthogonal trusses with varying thickness, and show that

^{*}Institute for Applied Mathematics, Rheinische Friedrich-Wilhelms-Universität Bonn, Endenicher Allee 60, 53115 Bonn, Germany

[†]Institute for Numerical Simulation, Rheinische Friedrich-Wilhelms-Universität Bonn, Endenicher Allee 60, 53115 Bonn, Germany

it leads to material composites with a compliance cost remarkably close to the optimal composite obtained from sequential lamination. Numerical experiments with different simple, parametrized geometries in the microscopic cells were performed in [21], and have lead to the identification of the rotated truss construction as the most promising candidate. Based on this two-scale approach for the elastic state equation one can optimize the parameters controlling the microscopic pattern, i. e., the two width parameters of the trusses and the rotation angle, considered as functions of the macroscale position. Numerical results suggest that the parameter functions controlling the microscopic patterns are smooth in large regions of the elastic workpiece. At the same time, in small regions the simple model for the microscopic supporting structure tends to show more complex patterns.

Related work. Shape optimization in general is a well-established field and covered extensively in the literature, see e. g. the textbooks [13, 3]. Regarding the theory of homogenization we refer to [35, 15, 20, 17, 18, 44]. The foundations for the sequential laminates construction were already laid early in [53, 47, 28, 43, 30, 6]. In [1] laminates were used to develop a practical numerical scheme for the optimization of the material composition in mechanical work pieces. Further optimal microstructures include concentric spheres for hydrostatic loads [32], confocal ellipsoids [31], and the Vigdergauz construction [56]. We refer to [18, 44] for a more complete discussion.

Very similar to our two-scale approach with parametrized microstructures [21] is the earlier work by Barbarosie and Toader. Based on optimization of holes in generalized periodic domains for given macroscopic affine displacements [7, 8] they set up a macroscopic finite element scheme in [9] working with effective material properties evaluated via numerical homogenization. Both methods are in line with the heterogeneous multi-scale method (HMM) [26, 24, 25, 27], a general paradigm to tackle numerical problems involving different length scales. Another method related to the optimization of microscopic geometries is the free material optimization approach [33]. In this case one first optimizes the coefficients of the effective elasticity tensor, and then in a post-processing step one searches for approximating microscopic realizations.

A posteriori error estimates for elliptic homogenization problems with fine scale diffusion were derived in the context of HMM in [50, 34]. In contrast to classical discretization error estimates it is however often required to assess the error w. r. t. a certain cost functional. Such goal-oriented error estimates for quantities of interest of a real composite work piece were derived in [51, 48, 49, 54]. In this contribution we follow the dual weighted residual (DWR) method [12], see e. g. [11] in particular for optimal control problems. This approach has recently been put to work for a variety of different applications. See [10] for a quasi-optimality result of the adaptive finite element scheme using a special marking strategy, [14, 55, 42] for the treatment of control and state constraints, and [40] for matrix valued L^1 optimal control. A posteriori error estimates in the context of shape optimization have been studied in [39] for a tracking type cost functional and Helmholtz state equation, in [45, 46], where DWR is used to assess the PDE error while the geometric error estimates relate to the Laplace Beltrami operator, and in [37, 38] for one shot methods applied to fuel ignition problems and aerodynamic shape optimization. In [16] error estimation for the optimal design in the context of Navier Stokes flow is discussed and in [59] estimates for the variable thickness sheet model are derived. In [29] a posteriori error estimates have been derived for shape optimization in a two-scale context with nested laminates on the microscale. To this end, the dual weighted residual approach has been applied leading to an associated adaptive meshing strategy.

The paper is organized as follows. In Section 2 we will briefly address the fundamental concepts of linearized elasticity, shape optimization w. r. t. the compliance objective and optimal material composites attained by the sequential lamination construction. Furthermore, we briefly review the numerical two-scale model in linearized elasticity. The dual weighted residual approach for the compliance cost is developed in Section 3. In the resulting estimates, as usual, certain weights still involve the continuous solution of the state equation. A suitable numerical approximation which enables to derive effective local error indicators is presented in Section 4. Some comments on the implementation are given in Section 5 and in Section 6 we present our numerical results.

2 Optimization of material composites

In this section we will briefly revise the fundamental concepts of linearized elasticity, shape optimization with the compliance objective and optimal microstructures given by sequential lamination. Furthermore, we will introduce a two-scale approach for the elastic behavior of microstructured materials, where the microstructure is given by a parametrized truss construction.

Linearized elasticity. Let us assume that an elastic workpiece is described by a simply connected domain $D \subset \mathbb{R}^2$ with Lipschitz boundary ∂D . Suppose that the boundary is split into a fixed relatively open subset Γ_D , a Dirichlet part where the displacement vanishes, and $\Gamma_N := \partial D \setminus \Gamma_D$, a Neumann part where sufficiently regular surface loads g can be applied. Then the induced displacement $u[C]$ is the unique solution $u : D \rightarrow \mathbb{R}^2$ of the partial differential equations of linearized elasticity, given in variational form as

$$a(C; u, \varphi) = l(\varphi) \quad \forall \varphi \in H_{\Gamma_D}^1 \quad (1)$$

with the quadratic form $a(C; u, \varphi) := \int_D C(x) \varepsilon[u] : \varepsilon[\varphi] \, dx$ and the linear form $l(\varphi) := \int_{\Gamma_N} g \cdot \varphi \, da(x)$. Here $H_{\Gamma_D}^1$ denotes the Sobolev space of L^2 vector-valued functions with weak derivatives in $L^2(D)$ and vanishing trace on Γ_D , $\varepsilon[u] := \frac{1}{2} (Du + Du^\top)$ denotes the symmetrized strain tensor with the Jacobian Du , ν the outward pointing normal on Γ_N and $C \in L^\infty(D, \mathbb{R}^{2^4})$ the elasticity tensor. Furthermore, $(C\epsilon)_{ij} = \sum_{kl} C_{ijkl} \epsilon_{kl}$ and $\sigma : \epsilon = \sum_{ij} \sigma_{ij} \epsilon_{ij}$ for two matrices $\sigma, \epsilon \in \mathbb{R}^{2 \times 2}$. The fourth order tensor $C(x)$ characterizes the material properties at each point $x \in D$ and will later be given by the effective tensor arising either from the explicit homogenization formula for laminate microstructures or from the solution of the microscopic cell problem. As usual, we assume that C fulfills the symmetry properties $C_{ijkl} = C_{jikl} = C_{ijlk} = C_{klij}$ and the ellipticity condition $C \xi : \xi \geq c |\xi + \xi^\top|^2$.

Shape optimization. We consider a cost functional $J[C, u]$ which we aim at minimizing under the constraint that u solves the associated elastic problem (1). In our numerical application, we adopt the classical compliance optimization approach to shape optimization. This means that we optimize the rigidity of an object by minimizing the elastic energy, or compliance, given by the functional

$$J[C, u] := \int_{\Gamma_N} g \cdot u \, da(x) = l(u), \quad (2)$$

which actually does not depend on C . However, from (1) one obtains $J[C, u[C]] = a(C; u[C], u[C])$. The shape optimization problem now amounts to finding a subset $\Omega \subset D$ where a hard material with elasticity tensor A should be placed. The remaining part $D \setminus \Omega$ is either left void or filled with a weak material with elasticity tensor B , so that the actual elasticity tensor is given by $C = \chi_\Omega A + (1 - \chi_\Omega)B$, where $\chi \in L^\infty(D, \{0, 1\})$ is the characteristic function of Ω . Throughout this paper we only consider isotropic materials that are described by the two Lamé parameters λ and μ . If the amount of hard material is constrained, i.e. $\int_D \chi_\Omega \, dx = \Theta$ with $\Theta > 0$ fixed, the resulting minimization problem is ill-posed and the formation of microstructures can be observed in numerically computed minimizing sequences.

Sequential lamination. To recover well posedness the minimization problem can be relaxed by allowing material of intermediate density at each point, i.e. $\chi \in [0, 1]$. The theory of homogenization then permits to compute the effective material properties C^* of mixtures of the constituents A and B on different underlying length scales. We will refer to the literature for details [3, 20, 44]. Most important for our exposition here is the fact that a sequential lamination construction yields effective materials that attain lower bounds on the local elastic energy density, called Hashin-Shtrikman bounds, and thus represent optimal microstructures. They are obtained by layering hard and soft material along a certain direction with a certain ratio, computing homogenized elastic properties and using those to iterate the construction on a subsequent, substantially larger length scale, see the sketch in Figure 1. For the compliance objective in two space dimensions



Figure 1: Sketch of twofold sequential lamination. Freely rotated cells with rectangular holes (see dotted red marking) representing orthogonal trusses (see red marking).

two iterations of the lamination construction are indeed sufficient and the parameters of the construction (direction of the lamination, volume fraction of each phase, and overall local density) can explicitly be computed from the local stress $\sigma(x) = C^*(x)\varepsilon[u(x)]$. At the same time the effective material properties can likewise be computed explicitly from the parameters, leading to an alternating algorithm for computing globally optimal relaxed shapes. It is moreover possible to ultimately pass from the weak material B to void. For further details we refer to [41, 4, 2, 1].

A two-scale approach for approximating microstructures. In this paper, we aim at the numerical computation of a near optimal material composite which consists of a mechanically constructible and simple microstructure, based on a microscopic pattern of two rotated, orthogonal trusses of different width, cf. Figure 1. To this end, assume that the microstructure of the two orthogonal, rotated trusses is parametrized via the (relative) width δ_1 and δ_2 of the two trusses ($0 < \delta_1, \delta_2 < 1$) and the rotation angle α . The vector of parameters is denoted by $q = (\alpha, \delta_1, \delta_2)$ and depends on the macroscopic position x , $q(x) := (\alpha(x), \delta_1(x), \delta_2(x))$. We then define the microscopic pattern on the (periodically extended) fundamental cell $\omega[q(x)] := Q(\alpha(x))(-\frac{1}{2}, \frac{1}{2})^2$ of a periodic lattice at the position x , with $Q(\alpha)$ denoting the rotation by the angle α . In fact, the cell $\omega[q(x)]$ splits into a domain $\omega_A[q(x)]$ with hard material described by the elasticity tensor A and a remaining domain $\omega_B[q(x)] := \omega[q(x)] \setminus \omega_A[q(x)]$ with soft material described by the elasticity tensor B . The hard phase is given by

$$\omega_A[q(x)] := Q(\alpha(x)) \left(\left[-\frac{\delta_1(x)}{2}, \frac{\delta_1(x)}{2} \right] \times \left[-\frac{1}{2}, \frac{1}{2} \right] \cup \left[-\frac{1}{2}, \frac{1}{2} \right] \times \left[-\frac{\delta_2(x)}{2}, \frac{\delta_2(x)}{2} \right] \right).$$

Let us remark that in the implementation of the boundary element method used to solve the microscopic correction problem it is advantageous to consider a shifted fundamental cell $\tilde{\omega}[q(x)]$ resulting from a shift on the periodic lattice by $\frac{1}{2}Q(\alpha(x))(1, 1)$, with the splitting $\tilde{\omega}_B[q(x)] = Q(\alpha(x)) \left(\left[\frac{\delta_1(x)}{2}, 1 - \frac{\delta_1(x)}{2} \right] \times \left[\frac{\delta_2(x)}{2}, 1 - \frac{\delta_2(x)}{2} \right] \right)$ and $\tilde{\omega}_A[q(x)] = \tilde{\omega}[q(x)] \setminus \tilde{\omega}_B[q(x)]$ which describe the identical periodic, microscopic pattern (cf. dotted red line in Figure 1) with a single interface. Given this splitting of the fundamental cell the variational form of the two-scale state equation reads as follows: For given isotropic constituents A and B and admissible locally periodic perforations on the microscale, find an effective macroscopic displacement $u^* \in H_{\Gamma_D}^{1,2}$ and a periodic microscopic correction $w^* \in \mathbf{W}_\alpha$ solving the two-scale equation

$$\int_D \int_{\omega[\alpha(x)]} C(x, y)(\varepsilon[u^*(x)] + \varepsilon[w^*(x, y)]) : (\varepsilon[\phi(x)] + \varepsilon[\psi(x, y)]) \, dy \, dx = \int_{\Gamma_N} g(x) \cdot \phi(x) \, da(x)$$

for all $\phi \in H_{\Gamma_D}^{1,2}$ and all functions $\psi \in \mathbf{W}_\alpha$, where the function space of microscopic periodic displacement corrections is defined as

$$\mathbf{W}_\alpha := \left\{ \psi : (x, y) \mapsto \psi(x, y) \in \mathbb{R}^2 \text{ where} \right. \\ \left. x \in D, y \in \omega[\alpha(x)], \psi(x, y + z) = \psi(x, y) \, \forall z \in Q(\alpha(x))\mathbb{Z}^2, \|\psi\|_{\mathbf{W}_\alpha} \leq \infty \right\}$$

with $\|\psi\|_{\mathbf{W}_\alpha} := \left(\int_D \int_{\omega[\alpha(x)]} \psi(x, y)^2 + |D_y \psi(x, y)|^2 \, dy \, dx \right)^{\frac{1}{2}}$. Here, $C(x, y) = A$ for $y \in \omega_A[q(x)]$ and $C(x, y) = B$ for $y \in \omega_B[q(x)]$. Concerning the underlying two-scale methodology we refer to

[27]. Equivalently the problem can be rewritten on the macroscale as in (1) with $C(x)$ replaced by the effective elasticity tensor $C^*[q](x)$ which is defined variationally via

$$C^*(x) \varepsilon[u(x)] : \varepsilon[u(x)] = \int_{\omega[\alpha(x)]} C(x, y) \varepsilon[R^*[u](x, y)] : \varepsilon[R^*[u](x, y)] \, dy \quad (3)$$

with the reconstruction $R^*[u](x, y) := u(x) + w(x, y)$ for w defined as the (up to constant translations unique) solution of the correction problem

$$\int_{\omega[\alpha(x)]} C(x, y) (\varepsilon[u(x)] + \varepsilon[w(x, y)]) : \varepsilon[\psi(x, y)] \, dy = 0 \quad \forall \psi \in \mathbf{W}_\alpha.$$

Indeed, based on (3) and the symmetry assumption for the effective elasticity tensor we get

$$C_{ijkl}^* = C^* \varepsilon_{ij} : \varepsilon_{kl} = C^* \varepsilon_{ij+kl} : \varepsilon_{ij+kl} - C^* \varepsilon_{ij-kl} : \varepsilon_{ij-kl} \quad (4)$$

with $\varepsilon_{ij} = \frac{1}{2}(e_i \otimes e_j + e_j \otimes e_i)$ and $\varepsilon_{ij \pm kl} = \frac{1}{2}(\varepsilon_{ij} \pm \varepsilon_{kl})$ where $e_1 = (1, 0)$ and $e_2 = (0, 1)$.

Macroscopic and microscopic discretization. To discretize the problem we assume the macroscopic domain D to be polygonally bounded and equipped with an admissible and regular finite element mesh \mathcal{M}_h , cf. [19], with elements $E \in \mathcal{M}_h$ and a piecewise constant mesh size function h . In our implementation, we assume that D can be meshed with a rectangular mesh and use a finite element ansatz for the discrete elastic displacement u_h on the macroscale in the finite element space \mathcal{V}_h of piecewise bi-quadratic and continuous vector-valued functions with vanishing trace on Γ_D . As for the elastic material properties we consider a piecewise constant tensor field C_h^* , derived either from a set of parameters describing sequential lamination or from microscopic perforation in the two-scale model. We then compute the solution u_h of the discrete weak problem $a(C_h^*; u_h, \varphi_h) = l(\varphi_h)$ for all $\varphi_h \in \mathcal{V}_h$.

In case the effective material properties C_h^* are not given explicitly, as in our case of the rotated trusses, they have to be computed numerically by solving the cell problem (3). To this end, we employ a boundary element method for which only the boundaries of the perforated unit cell $\omega_A[q(x)]$ need to be discretized by polygon arcs. Let us mention here that this microscopic mesh is discretized uniformly and will not undergo any refinement. The boundary element method requires to deal with the fundamental solution of the linearized elasticity PDE. Here we choose as the underlying material model the Lamé Navier model for an isotropic material, see e.g. [52],

$$u_{ki}^*(x, y) = \frac{\lambda + \mu}{4\pi(\mu(\lambda + 2\mu))} \left(-\delta_{ki} \frac{\lambda + 3\mu}{\lambda + \mu} \log \|x - y\| + \frac{(y_k - x_k)(y_i - x_i)}{\|x - y\|^2} \right),$$

where λ and μ are the Lamé parameters that will both be set to 1 for our numerical computations. The fundamental solution is used to rewrite the elasticity equation as a boundary integral equation leading to

$$w = U[A\varepsilon[w] \cdot \nu] - V[w], \quad (5)$$

where the boundary integral operators U and V are the single and double layer operator, respectively. On the discretized boundary a set of collocation points ξ_i is fixed and the displacement w as well as the normal tension $A\varepsilon[w] \cdot \nu$ is approximated by linear interpolation of nodal values at ξ_i . Equation (5) now has to hold for every ξ_i leading to a linear system of equations. The boundary integral operators U and V are only applied to piecewise affine functions on the boundary, therefore their application to the basis functions has been computed analytically. As we typically consider mixed boundary value problems equation (5) has to be rearranged according to known and unknown values. Further details can be found in [5].

The coefficients of the effective material tensor can then be evaluated as in (3) using a boundary integral formulation. Likewise it is possible to derive a shape gradient, cf. [22], to be able to compute sensitivities $\nabla_{q(x)} C_{ijkl}^*$ of the elastic coefficients w. r. t. the describing microscopic parameters. It is then used in the optimization scheme for the minimization of the macroscopic cost functional (2). Let us mention that deriving the cost functional initially also leads to sensitivities of the elastic solution w. r. t. $q(x)$. We use as usual the associated Lagrangian approach and derive the adjoint equation to compute the gradient of the cost functional. For further details we refer to the earlier work [21]. In Section 5 we will give further details on the implementation.

3 Modeling and discretization estimate

In what follows we will derive an estimate for the difference of the achievable compliance cost using the numerical two-scale model with a macroscopically parametrized microscopic pattern of two rotated, orthogonal trusses and the optimal compliance cost associated with the nested laminate construction. This estimate reflects both the modeling error caused by the choice of the mechanically constructible but non optimal microscopic pattern and the numerical discretization error. Let us emphasize that we do not expect that the resulting difference of compliance costs vanishes for the mesh size tending to zero. In fact, we are interested in the remaining global modeling error and its associated spatial distribution. Furthermore, we will use the resulting error estimate to adapt the macroscopic finite element mesh.

Let u^L be the solution of the continuous problem (1) involving the optimal elasticity tensor field C^L resulting from an optimal sequentially laminated microstructure at each point. Likewise let u_h^S be the discrete macroscopic solution when using the two-scale model with piecewise constant effective tensors C_h^S obtained by solving the cell problems (3) for a pattern of two rotated, orthogonal trusses. Ultimately we are interested in an estimate of the corresponding difference of compliance cost values

$$|J[C^L; u^L] - J[C_h^S; u_h^S]|,$$

in particular for C_h^S being the field of elasticity tensors resulting for the optimal choice of the microstructure parameters and for u_h^S computed as the resulting discrete macroscopic strain in the finite element space \mathcal{V}_h . To derive such an estimate we employ the dual weighted residual approach [11] for optimal control problems. Here, the controls—which have to reside in the same space—are the coefficient functions of the elasticity tensors C^L, C_h^S . Using the usual notation $\|\cdot\|_{m,p,A}$ for the $W^{m,p}$ Sobolev norm on a set A we obtain the following theorem.

Theorem 3.1 (Weighted a posteriori modeling error estimate). *Given the continuous solution u^L to (1) for an optimal effective elasticity tensor field C^L (as obtained from optimal nested lamination) and the macroscopic finite element solution u_h^S for the two-scale model with a piecewise constant tensor field C_h^S we obtain for the difference of the associated compliance cost values the estimate*

$$|J[C^L, u^L] - J[C_h^S, u_h^S]| \leq \sum_E \eta_E(u^L, C^L, u_h^S, C_h^S) + \mathcal{R}, \quad (6)$$

where the cellwise η_E values are decomposed as follows

$$\begin{aligned} \eta_E(u^L, C^L, u_h^S, C_h^S) &:= \eta_E^u + \eta_{\partial E}^u + \frac{1}{2}\eta_E^C \quad \text{with} \\ \eta_E^u &:= \left| \int_E \operatorname{div} \{C_h^S \varepsilon[u_h^S]\} \cdot (u^L - u_h^S) \, dx \right|, \\ \eta_{\partial E}^u &:= \left| \int_{\partial E} j(C_h^S \varepsilon[u_h^S]) \cdot (u^L - u_h^S) \, da(x) \right|, \\ \eta_E^C &:= \left| \int_E (C^L - C_h^S) \varepsilon[u_h^S] : \varepsilon[u_h^S] \, dx \right|, \end{aligned}$$

and j denotes the jump of the normal stress across an edge. Furthermore, the remainder is given by

$$\mathcal{R} := \frac{1}{2}a(e_C; e_u, e_u)$$

and is thus of higher order in the difference of states $e_u := u^L - u_h^S$ and the difference of elasticity tensors $e_C := C^L - C_h^S$.

Proof. The proof follows the usual procedure for deriving dual weighted residual estimates (cf. [11] for the method in general or [29] for a shape optimization problem based on microscopic sequential lamination). We consider the Lagrangian

$$\tilde{\mathcal{L}}(C, u, p) := J[C, u] + a(C; u, p) - l(p) \quad (7)$$

for arbitrary C , u , and p . The newly introduced function p represents the solution to an adjoint equation. In case of the compliance cost functional it is, however, trivially determined by $p = -u$, cf. [3]. According to our assumption u^L and u_h^S solve the continuous and the discrete state equation for given C^L and C_h^S , respectively. Thus, we obtain $a(C^L; u^L, -u^L) - l(-u^L) = 0$, $a(C_h^S; u_h^S, -u_h^S) - l(-u_h^S) = 0$, which implies

$$e_{\mathcal{L}} := \tilde{\mathcal{L}}(C^L, u^L, -u^L) - \tilde{\mathcal{L}}(C_h^S, u_h^S, -u_h^S) = J[C^L, u^L] - J[C_h^S, u_h^S]. \quad (8)$$

Thus, we focus on the error in the Lagrangian involving the tensor fields C^L , C_h^S and the corresponding primal solutions u^L , u_h^S . We use the shortcut notation $\mathcal{L}(C, u) := \tilde{\mathcal{L}}(C, u, -u)$.

To derive a first order expansion of $e_{\mathcal{L}}$ we interpolate linearly between the quantities of the continuous lamination and the discrete two-scale problem and obtain for the difference in the Lagrangian

$$e_{\mathcal{L}} = \int_0^1 \frac{d}{ds} \mathcal{L}(C_h^S + se_C, u_h^S + se_u) ds.$$

We define $f(s)$ as the above integrand, i.e. $f(s) := \frac{d}{ds} \mathcal{L}(C_h^S + se_C, u_h^S + se_u)$, and apply the trapezoidal rule $\int_0^1 f(s) ds = \frac{1}{2}(f(0) + f(1)) - \frac{1}{2} \int_0^1 f''(s) s(1-s) ds$. All derivatives exist and can be explicitly calculated, since \mathcal{L} is a polynomial in its arguments, but it is convenient to do this only at the final stage of the computation. From the assumption that C^L is the optimal field of elasticity tensors and u^L the associated primal elastic solution we deduce that $(C^L, u^L, -u^L)$ is a stationary point of the Lagrangian. Thus, we obtain that

$$f(1) = \nabla \mathcal{L}(C^L, u^L) \cdot (e_C, e_u)^\top = 0.$$

Hence, using the remainder term $\mathcal{R} := -\frac{1}{2} \int_0^1 \frac{d^3}{ds^3} \mathcal{L}(C_h^S + se_C, u_h^S + se_u) s(1-s) ds$ we end up with the following representation of the difference of compliance cost values:

$$e_{\mathcal{L}} = \frac{1}{2} \mathcal{L}_{,u}(C_h^S, u_h^S)(u^L - u_h^S) + \frac{1}{2} \mathcal{L}_{,C}(C_h^S, u_h^S)(C^L - C_h^S) + \mathcal{R}. \quad (9)$$

Next, we decompose the first two terms into contributions on the elements and element boundaries of the macroscopic finite element mesh and obtain using integration by parts

$$\begin{aligned} & \mathcal{L}_{,u}(C_h^S, u_h^S)(u^L - u_h^S) \\ &= -2 \int_D C_h^S \varepsilon[u_h^S] : \varepsilon[u^L - u_h^S] dx + 2 \int_{\Gamma_N} g \cdot (u^L - u_h^S) da(x) \\ &= 2 \sum_E \left(\int_E \operatorname{div} \{C_h^S \varepsilon[u_h^S]\} \cdot (u^L - u_h^S) dx - \int_{\partial E} C_h^S \varepsilon[u_h^S] n \cdot (u^L - u_h^S) da(x) \right. \\ & \quad \left. + \int_{\partial E \cap \Gamma_N} g \cdot (u^L - u_h^S) da(x) \right) \\ &\leq 2 \sum_E (\eta_E^u + \eta_{\partial E}^u) \end{aligned} \quad (10)$$

with the postulated residual terms $\eta_E^u = |\int_E \operatorname{div} \{C_h^S \varepsilon[u_h^S]\} \cdot (u^L - u_h^S) dx|$ and $\eta_{\partial E}^u = |\int_{\partial E} j(C_h^S \varepsilon[u_h^S]) \cdot (u^L - u_h^S) da(x)|$. Thereby, $j(\sigma)(x) = [\sigma(x) \cdot \nu(x)]$ on interior edges, $j(\sigma)(x) = \sigma(x) \cdot \nu(x) - g(x)$ on Γ_N , and $j(\sigma)(x) = 0$ on Γ_D . Here, $[\sigma(x) \cdot \nu(x)]$ denotes the jump of the normal stress across an edge, i.e. $[\sigma(x) \cdot \nu(x)] = (\sigma(x)|_E - \sigma(x)|_{E'}) \cdot \nu(x)$ for $x \in E \cap E'$, and ν being the normal on $E \cap E'$ pointing from E to E' . For the second term in (9) we obtain the straightforward splitting

$$\mathcal{L}_{,C}(C_h^S, u_h^S)(C^L - C_h^S) = - \int_D (C^L - C_h^S) \varepsilon[u_h^S] : \varepsilon[u_h^S] dx \leq \sum_E \eta_E^C. \quad (11)$$

Finally, $\frac{d^3}{ds^3} \mathcal{L}(C_h^S + se_C, u_h^S + se_u) = -6a(e_C; e_u, e_u)$ does not depend on s , and a straightforward integration concludes the proof. \square

Let us remark that the first two terms in the definition of η_E (i.e. $\eta_E^u + \eta_{\partial E}^u$) measure the discretization error. Indeed, η_E^u and $\eta_{\partial E}^u$ include the element and the singular residual of the primal problem along with weighting terms. They both are expected to vanish for the mesh size tending to 0. The last term represents the difference of the stored elastic energy $\mathcal{E}[C, u] = \frac{1}{2} \int_D C \varepsilon[u] : \varepsilon[u] \, dx$ for the different elasticity tensors C^L and C_h^S evaluated for the discrete strain u_h^S . This term measures the modeling error and is not required to vanish in general.

4 Derivation of effective local error indicators

The cellwise values η_E of the weighted a posteriori error estimate in Theorem 3.1 depend on the computed numerical solution u_h^S and on the unknown, continuous displacement field u^L corresponding to the as well unknown, optimal elasticity tensor field C^L . Furthermore, the energy difference terms η_E^C involve the optimal continuous elasticity tensor C^L . In order to make practical usage of this estimate we need to compute suitable approximations of the weighting terms $(u^L - u_h^S)$ and to efficiently estimate the locally optimal effective elasticity tensor C^L . Based on these approximations we then replace η_E by a computable approximation. This can then in the fully practical algorithm be used to steer the grid refinement and to evaluate a distribution of the modeling error due to the replacement of the nested lamination microstructure by the microstructure consisting of rotated, orthogonal trusses.

Approximation of u^L . On a given mesh \mathcal{M}_h let us consider a two-scale model, where the effective discrete macroscopic strain $u_h \in \mathcal{V}_h$ in the Galerkin approximation of (1) on \mathcal{M}_h results from a microscopic nested laminate construction. We denote by C_h^L and u_h^L the optimal effective elasticity tensor and strain resulting from a minimization of the compliance cost functional. Thereby, we take into account discrete tensor fields which are piecewise constant on the elements of the mesh. It is well-known that the C_h^L can be easily retrieved from the corresponding stress field $\sigma_h = C_h^L \epsilon[u_h^L]$. Indeed, the lamination directions coincide with the eigendirections of σ_h and based on this insight the optimal ratios between the two materials in each involved lamination of the local composite can be easily identified as functions of the eigenvalues of the stress σ_h (for details we refer to [3]). Altogether, we obtain

$$C_h^L = \mathbf{C}(\alpha(\sigma_h), \lambda_1(\sigma_h), \lambda_2(\sigma_h)) \quad (12)$$

for some function

$$\mathbf{C} : \mathbb{R}^3 \rightarrow \mathbb{R}^{2^4}; \alpha, \lambda_1, \lambda_2 \mapsto \mathbf{C}(\alpha, \lambda_1, \lambda_2),$$

which maps the rotation angle α from the canonical basis into the basis of the eigendirections of the stress and the two eigenstresses λ_1 and λ_2 to the effective elasticity tensor of the optimal nested laminate associated with the corresponding underlying elastic stress. For the detailed derivation of this function we refer to [3]. In Section 5 we give the explicit formulas. Equation (12) gives rise to a simple iterative minimization algorithm starting from some initial strain. Indeed, given $u_{h,i-1}^L$ one first evaluates

$$C_{h,i}^L = \mathbf{C}(\alpha(\sigma_{h,i}), \lambda_1(\sigma_{h,i}), \lambda_2(\sigma_{h,i}))$$

with $\sigma_{h,i} = C_{h,i-1}^L \epsilon[u_{h,i-1}^L]$ and then computes $u_{h,i}^L$ as the discrete solution of the Galerkin approximation of (1) with the elasticity tensor $C_{h,i}^L$ in \mathcal{V}_h . As a suitable initial elasticity tensor and strain field we consider C_h^S and u_h^S , respectively. Then, we compute for some fixed $k \in \mathbb{N}$ the elasticity tensor $C_{h,k}^L$ and the associated strain $u_{h,k}^L$.

Following the usual procedure in the context of the dual weighted error estimation approach we now use a higher order interpolation of a discrete PDE solution in a neighborhood of each cell as a higher order approximation for the continuous PDE solution and apply this to $u_{h,k}^L$. Specifically, for a cell E of an adaptive mesh \mathcal{M}_h we proceed as follows. Let us assume that \mathcal{M}_h is generated based on an adaptive quadtree data structure and that E is one of the four child cells of a coarser cell E^c . Now, we consider the Lagrangian interpolation $\mathcal{I}_h^{(4)}$ on the space of bi-quartic polynomials

based on functional evaluation on the union of bi-quadratic Lagrangian nodes on the children of E^c . Given $u_{h,k}^L$ we define $\tilde{u}_{h,k}^L$ on the cell E as $\mathcal{I}_h^{(4)} u_{h,k}^L|_E$. With $\tilde{u}_{h,k}^L$ at hand, we can define the approximations

$$\tilde{\eta}_E^u = \left| \int_E \operatorname{div} \{ C_h^S \varepsilon[u_h^S] \} \cdot (\tilde{u}_{h,k}^L - u_h^S) \, dx \right|, \quad \tilde{\eta}_{\partial E}^u = \left| \int_{\partial E} j(C_h^S \varepsilon[u_h^S]) \cdot (\tilde{u}_{h,k}^L - u_h^S) \, da(x) \right|, \quad (13)$$

which can be computed based on a Gaussian (tensor product) quadrature with order 5 and 3×3 nodes, respectively.

Approximation of C^L . The stress tensor σ is uniquely determined by the rotation angle α and its two eigenvalues λ_1 and λ_2 , i. e.

$$\sigma = R(\alpha) \begin{pmatrix} \lambda_1 & 0 \\ 0 & \lambda_2 \end{pmatrix} R(\alpha)^T,$$

where $R(\alpha)$ is the rotation from the canonical basis into the basis of the eigenstrains. On the other hand $\sigma = C^L \varepsilon[u^L]$ with $C^L = \mathbf{C}(\alpha, \lambda_1, \lambda_2)$. Hence, we define a function

$$F(\alpha, \lambda_1, \lambda_2) = \mathbf{C}(\alpha, \lambda_1, \lambda_2) \varepsilon[u^L] - R(\alpha) \begin{pmatrix} \lambda_1 & 0 \\ 0 & \lambda_2 \end{pmatrix} R(\alpha)^T, \quad (14)$$

which maps the three parameters $\alpha, \lambda_1, \lambda_2$ to a symmetric 2×2 matrix with its three degrees of freedom. Roots of this function correspond to stresses σ and elasticity tensors C^L for a given strain tensor $\varepsilon[u^L]$ in the optimal laminate configuration. In the implementation we use Newton's method to compute for given $\varepsilon[\tilde{u}_{h,k}^L]$ a root $(\alpha, \lambda_1, \lambda_2)$ of F . Thus, we obtain $\tilde{C}_{h,k}^L = \mathbf{C}(\alpha, \lambda_1, \lambda_2)$ as an admissible elasticity tensor corresponding to an optimal nested laminate microstructure for a given approximation $\tilde{u}_{h,k}^L$ of the optimal strain. Finally, based on $\tilde{C}_{h,k}^L$ we compute as an approximation of the local modeling error term η_E^C

$$\tilde{\eta}_E^C = \int_E (\tilde{C}_{h,k}^L - C_h^S) \varepsilon[u_h^S] : \varepsilon[u_h^S] \, dx \quad (15)$$

applying the above Gaussian (tensor product) quadrature of order 5.

Approximate evaluation of η_E . Taking into account the above approximation of the local weighting terms in $\tilde{\eta}_E^u, \tilde{\eta}_{\partial E}^u$ and the local modeling error term $\tilde{\eta}_E^C$, we obtain as an approximate upper bound for the difference $J[C^L, u^L] - J[C_h^S, u_h^S]$ in (6) the term $\sum_E \tilde{\eta}_E(u_h^S, C_h^S) + \mathcal{R}$ with

$$\tilde{\eta}_E(u_h^S, C_h^S) = \tilde{\eta}_E^u + \tilde{\eta}_{\partial E}^u + \frac{1}{2} \tilde{\eta}_E^C, \quad (16)$$

which is evaluated based on a given pair of discrete strain u_h^S and discrete elasticity tensor C_h^S , which correspond to the optimal compliance cost in the case of the microstructure formed by rotated, orthogonal trusses of varying width and rotation angle.

In what follows, we give some numerical evidence that an early truncation of the laminates algorithm already yields a sufficiently good approximation to the fully converged solution of the lamination model. In Figure 2 we show the absolute error in the compliance and the L^2 -error in the elastic solution for each iteration of the alternating lamination algorithm, see below, starting from the two-scale solution u_h^S corresponding to C_h^S . The difference is computed w. r. t. the final value at convergence, i. e. when subsequent compliance values differ by no more than 10^{-8} , of the lamination algorithm starting from the same initial values. In fact, we will use $k = 50$ iterations for our numerical computations.

5 Implementation

Our macroscopic computations are performed on an regular quadrilateral mesh implemented within the QuocMesh library¹. The library also provides a collocation type boundary element method for

¹<http://numod.ins.uni-bonn.de/software/quocmesh>

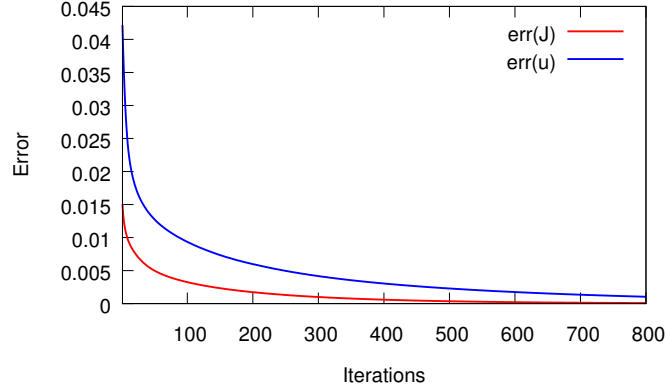


Figure 2: After each iteration of the laminates algorithm, starting from an initial state given by the two-scale model, the compliance objective and elastic solution are compared to the final state. The error in the compliance is the absolute value, the error in the elastic solution is the L^2 -error.

the solution of cell problems on the microscale. Furthermore it includes a classical Newton scheme using optimal step size control to solve (14). Adaptive refinements are realized via uniform subdivision and handling of constrained hanging nodes. As checkerboard instabilities are reported for the sequential lamination microstructure, cf. [36], we use bi-quadratic finite elements for stabilization on the macroscale. For numerical integration we use a Gauss quadrature rule of order 5 which turned out to be sufficient.

We reimplemented the alternating algorithm for sequential lamination microstructures suggested in [1] and already described in [29].

Given the rotation α of the dominant eigenvector of σ_h and its eigenvalues λ_1 and λ_2 , the lamination parameters and the effective elasticity tensor in equation (12) are explicitly given by

$$m[\sigma_h] = \frac{|\lambda_2(\sigma_h)|}{|\lambda_1(\sigma_h)| + |\lambda_2(\sigma_h)|}, \quad \theta[\sigma_h] = \min \left\{ 1, \sqrt{\frac{2\mu + \lambda}{4\mu(\mu + \lambda)l}} (|\lambda_1(\sigma_h)| + |\lambda_2(\sigma_h)|) \right\},$$

$$C_{mnop}^*[q] = R[\alpha] \bar{C}[m, \theta] := Q_{mi}[\alpha] Q_{nj}[\alpha] Q_{ok}[\alpha] Q_{pl}[\alpha] \bar{C}_{ijkl}[m, \theta],$$

$$\bar{C}_{1111}[m, \theta] = \frac{4\kappa\mu(\kappa + \mu)\theta(1 - \theta)(1 - m)(1 - m)}{4\kappa\mu m(1 - m)\theta^2 + (\kappa + \mu)^2(1 - \theta)}, \quad \bar{C}_{2222}[m, \theta] = \frac{4\kappa\mu(\kappa + \mu)\theta(1 - \theta)m}{4\kappa\mu m(1 - m)\theta^2 + (\kappa + \mu)^2(1 - \theta)},$$

$$\bar{C}_{1122}[m, \theta] = \frac{4\kappa\mu\lambda\theta^2 m(1 - m)}{4\kappa\mu m(1 - m)\theta^2 + (\kappa + \mu)^2(1 - \theta)}.$$

Here R is a linear mapping rotating the tensor \bar{C} given in reference configuration into the appropriate coordinate frame given by rotation parameter α . In its definition Q are 2×2 rotation matrices and the Einstein summation convention is used. The bulk modulus is defined as $\kappa = \lambda + \mu$ and l is a Lagrangian multiplier used in the alternating algorithm to enforce the volume constraint. The tensor \bar{C} is complemented using the symmetry relations and filling the remaining entries with 0. This yields a singular elasticity tensor that has to be regularized by adding a small constant.

Within each cell the underlying microstructure is specified by a small set of parameters leading to a finite dimensional constrained optimization problem solved by the open source software **Ipopt** [57, 58]. It implements an SQP type minimization scheme using limited memory BFGS updates to approximate the Hessian. To steer the adaptivity we follow a Dörfler strategy [23] marking cells giving rise to the top 40% of the total estimated error.

6 Numerical results

In the following we discuss the concrete application of our adaptive algorithm to four textbook examples of 2D shape optimization problems. For each of them we visualize the resulting solution

and refinement patterns and list the error indicator values and the computed cost values at each refinement step. As expected, the modeling error can not be reduced beyond a problem-dependent positive lower bound. In fact, after a substantial reduction of the discretization and the modeling error in the initial refinement stages, the algorithm builds an oscillatory pattern on the grid scale in certain regions. We discuss below the implications of these observations for the appropriate usage of the a posteriori error control.

The first scenario is a carrier plate modeled by a square domain $D = [0, 1]^2$ fixed at the bottom and subject to a uniform shearing load on the top, cf. Figure 3. The next scenario is a cantilever, cf. Figure 5. It is modeled by a rectangular domain $D = [0, 1] \times [0, 0.5]$, fixed at the left hand side and subject to a downwards pointing load located in the center of the right hand side. The third example is a bridge configuration given on the domain $D = [0, 1] \times [0, 0.5]$, cf. Figure 6. We prescribe roller boundary conditions on a small fraction of the lower boundary on the left and right hand side, i. e. only the vertical displacement component is kept fixed there. In between a uniform downwards pointing load is applied. Finally we consider an L-shaped domain $D = [0, 1]^2 \setminus [0.5, 1]^2$ fixed on top and subject to a downwards pointing load in the center of the lower right boundary, cf. Figure 7. All applied loadings have a magnitude of 1. For the cantilever scenario the global volume fraction is constrained to 50%, for all other scenarios to 67%, respectively.

For the carrier plate scenario we show the macroscopic computational domain at several steps of the adaptive scheme in Figure 3. Moreover the optimized microscopic geometries underlying each macroscopic element of the grid, the associated elementwise volume densities, and a color coding of the von Mises stress are shown. For the other scenarios we depict grid, visualization and von Mises stress of two intermediate refinement steps in Figures 5, 6, 7. To analyze the computed error indicators leading to the refined grids we list the contributions of each term for every refinement step in Tables 1 and 3. A striking observation is that the error indicator does not decrease at later stages of the adaptive algorithm. As noted earlier one cannot expect the indicator to go to zero due to the non vanishing modeling error. However, the tables show that while the modeling error increases at most mildly both discretization error terms show significant growth after a few refinement steps. In fact, this appears in regions where the stress tensor would indicate a nested laminate construction as the optimal local pattern. Thus, this locally optimal two-scale geometry cannot be realized by the rotated truss construction. As a compensation of this deficiency the algorithm seems to try to establish an additional intermediate scale via an oscillating pattern on the grid scale, which one clearly observes in the images, as for example in the last row of Figure 3, which shows a color coding of the local discretization error contributions. These oscillations have small effect on the energy but lead to significant additional discretization errors and therefore to the observed increase of the global discretization error estimate. Furthermore, these oscillations have an impact on the optimal compliance cost computed numerically on the various grids. This optimal cost depends on the discrete solution of the underlying constrained optimization problem and is characterized by a discrete saddle point of the Lagrangian (7). In particular, it increases if the elastic problem is not fully resolved, which is the case if the coefficients are rapidly varying. These discretization errors give rise to a substantial increase in the later refinement stages, as can be seen in the tables. The process seems to be self-propelling and propagating during subsequent refinement steps, resulting in refined computational domains that seem uneligible for the considered scenarios. As a comparison we show a refined grid after 24 refinement steps for the carrier plate scenario using the sequential lamination model from the earlier work [29] in Figure 4. Here one observes sharply resolved interfaces between regions of diverse material density. However, in the central gray domain where the optimal pattern is an actually nested laminate the grade of refinement keeps being moderate. The observed phenomenon does not stem from the adaptivity of the grid, as illustrated by the corresponding results based on four uniform refinement steps for the cantilever scenario, starting from the same initial grid as before. In Table 2 we again recognize the dominant increase of the discretization error terms.

In summary, our results illustrate good convergence of the objective functional and of the general structure of the two-scale shape. They also show that the modeling error can be reduced via the adaptive meshing strategy until a problem-dependent lower bound is approached. At this point the limit of the chosen microscopic model of the rotated trusses for the local shape pattern is obviously reached, as indicated by the necessity to construct an intermediate pattern via oscillations on the grid scale. The proposed a posteriori error bounds show a clear indication of this effect and allow to

stop the algorithm at that point. Extreme refinement appears to be neither necessary nor useful in the present setting. Without an additional regularity term in the cost functional which penalizes strong variations in the parameters of the microscopic patterns, the cost functional cannot be further reduced via a refinement of the grid, as observed in the tables. We also observe a clear coincidence of the increase in discretization error with the increase in the numerically computed cost value.

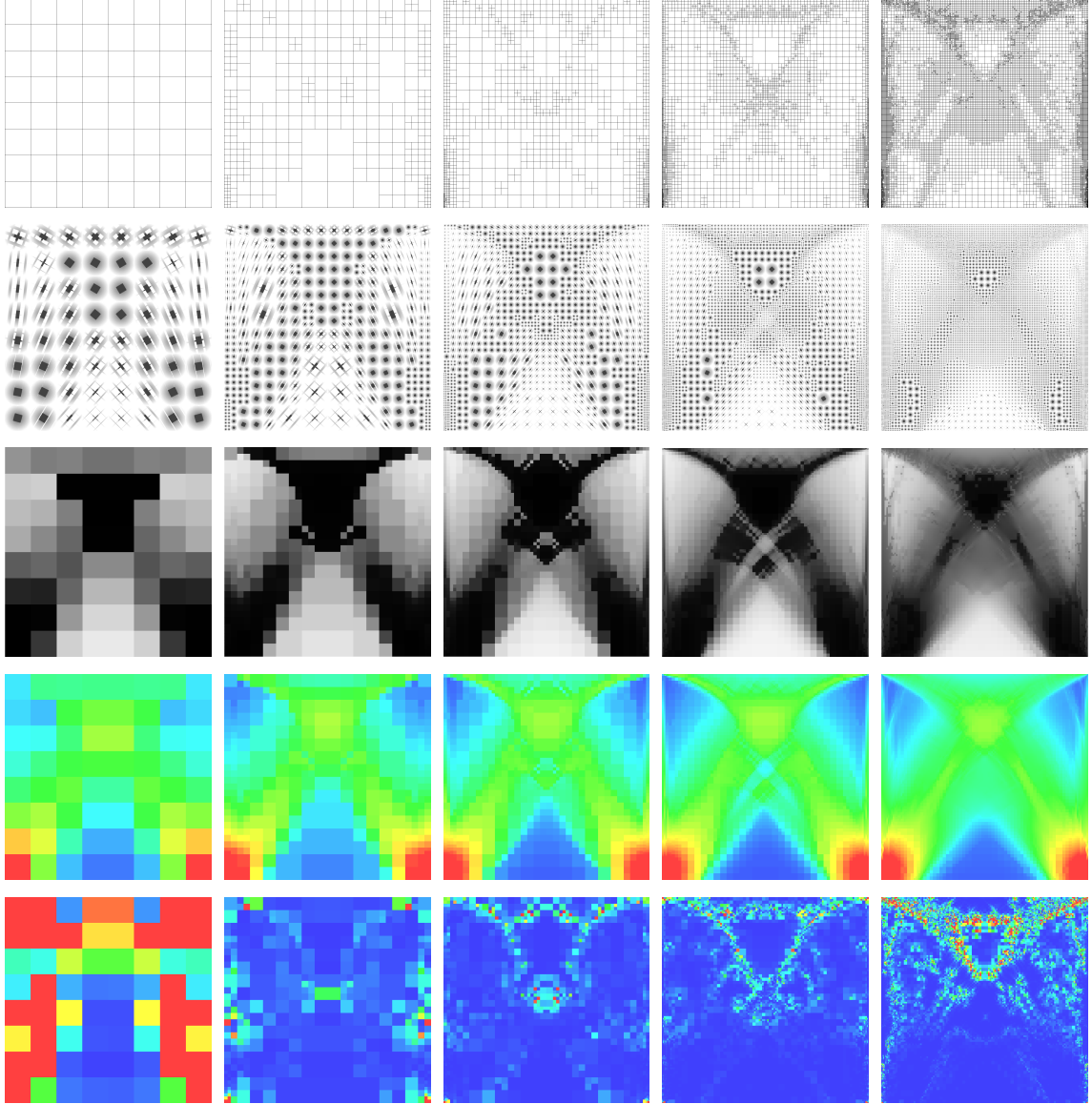
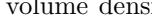


Figure 3: For the carrier plate scenario we depict from top to bottom: the adaptively refined grid after 0, 4, 7, 10, 13 refinement steps; a visualization of the optimized microstructure of the two-scale model using an iconic representation with the periodically extended perforations in white and the truss geometry on the fundamental cell in black on a uniformly gray background; the volume density on the elements of the macroscopic mesh; the von Mises stress color coded with  for values in $[0, 6]$, and the element wise error indicator $\tilde{\eta}_E^u + \tilde{\eta}_{\partial E}^u$ with the same color coding now for values in $[0, 0.4]$.

#Refs	Edge $\tilde{\eta}_{\partial E}^u$	Volume $\tilde{\eta}_E^u$	Model $\frac{1}{2}\tilde{\eta}_E^C$	Total $\tilde{\eta}_E(u_h^S, C_h^S)$	$J[C^S, u^S]$	#El
0	0.216758	0.371898	0.726425	1.315083	2.163037	64
1	0.089962	0.109742	0.496442	0.696147	2.142808	100
2	0.080205	0.107282	0.410473	0.597961	2.026496	154
3	0.045338	0.057250	0.355282	0.457871	2.006264	262
4	0.032952	0.030399	0.290097	0.353449	1.992369	382
5	0.024614	0.021315	0.216723	0.262653	1.941411	598
6	0.021418	0.022156	0.188472	0.232046	1.932662	868
7	0.020352	0.020339	0.165938	0.206630	1.906596	1318
8	0.019183	0.018444	0.140885	0.178513	1.901717	2077
9	0.020706	0.018520	0.128235	0.167461	1.890917	3241
10	0.022799	0.019582	0.107348	0.149730	1.898300	5002
11	0.026824	0.021944	0.096681	0.145451	1.901327	7576
12	0.031593	0.025283	0.100130	0.157007	1.914866	11365
13	0.052313	0.041381	0.129384	0.223079	1.933688	16903
14	0.079236	0.061311	0.151317	0.291865	1.952025	25558

Table 1: Components of the error indicator for the carrier plate scenario and each refinement step. The optimal compliance cost based on extrapolation of values obtained from a series of computations for the sequential lamination model on uniform grids is 1.83992. At steps 7 to 11 the value for the two-scale model differs from the optimal one by 2 to 3%.

#Refs	Edge $\tilde{\eta}_{\partial E}^u$	Volume $\tilde{\eta}_E^u$	Model $\frac{1}{2}\tilde{\eta}_E^C$	Total $\tilde{\eta}_E(u_h^S, C_h^S)$	$J[C^S, u^S]$	#El
0	0.216758	0.371898	0.726425	1.315083	2.163037	64
1	0.117318	0.131675	0.469026	0.718020	1.992764	256
2	0.026711	0.028785	0.374861	0.430358	1.922647	1024
3	0.010379	0.009895	0.207756	0.228032	1.903045	4096
4	0.004076	0.004095	0.220584	0.228756	1.945240	16384

Table 2: Components of the error indicator for the carrier plate scenario using uniform refinement.

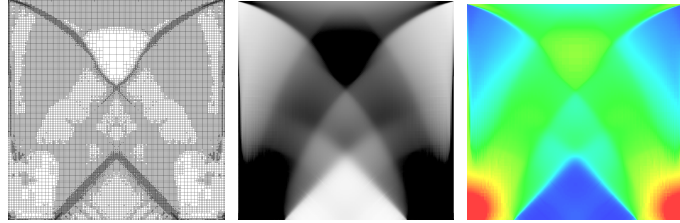


Figure 4: For comparison grid, density, and von Mises stress with color coding as in Figure 3 for values in $[0, 6]$ for the sequential lamination model after 24 refinement steps, based on the approach described in [29].

7 Conclusion

We presented a two-scale approach to shape optimization based on simple and physically realizable microstructures, consisting of two orthogonal trusses whose width and orientation are optimized. We gave a posteriori bounds of the resulting discretization and modeling error. We presented a numerical implementation of the scheme, based on the boundary element method at the microscale and finite elements at the macroscale, which uses the estimated error to guide grid adaptivity, and employed it to study several standard model problems in shape optimization.

Our results illustrate good convergence of the objective functional and of the general structure of the shape. However, after an initial decrease, the error indicator increases when the grid becomes finer and finer. This is attributed to the emergence of oscillations in the microscopic parameters at

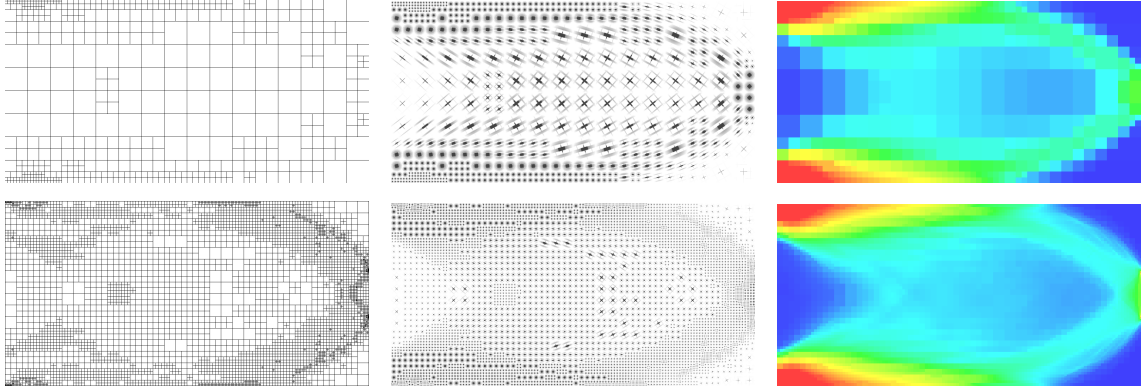


Figure 5: For the cantilever scenario after 4 / 9 refinement steps: adaptively refined grid; visualization of the two-scale model as in Figure 3; von Mises stress with color coding as in Figure 3 for values in $[0, 3]$.

#Refs	Cantilever			Bridge			L-Shape		
	$\tilde{\eta}_E^u + \tilde{\eta}_{\partial E}^u$	$\frac{1}{2}\tilde{\eta}_E^C$	$J[C^S, u^S]$	$\tilde{\eta}_E^u + \tilde{\eta}_{\partial E}^u$	$\frac{1}{2}\tilde{\eta}_E^C$	$J[C^S, u^S]$	$\tilde{\eta}_E^u + \tilde{\eta}_{\partial E}^u$	$\frac{1}{2}\tilde{\eta}_E^C$	$J[C^S, u^S]$
0	0.0243	0.0706	0.2416	0.7390	0.3552	0.9239	0.0668	0.0729	0.2848
1	0.0114	0.0503	0.2083	0.3058	0.3830	0.8466	0.0332	0.0508	0.2459
2	0.0068	0.0422	0.1924	0.2132	0.2909	0.7931	0.0206	0.0359	0.2270
3	0.0044	0.0324	0.1913	0.1011	0.2421	0.7632	0.0126	0.0322	0.2213
4	0.0049	0.0303	0.1889	0.0519	0.2139	0.7436	0.0088	0.0264	0.2198
5	0.0053	0.0250	0.1807	0.0413	0.2209	0.7355	0.0053	0.0239	0.2190
6	0.0050	0.0220	0.1772	0.0436	0.2620	0.7354	0.0088	0.0213	0.2147
7	0.0067	0.0182	0.1761	0.3006	0.4511	0.8585	0.0108	0.0221	0.2113
8	0.0111	0.0218	0.1776	0.0804	0.3054	0.7570	0.0185	0.0291	0.2123
9	0.0164	0.0242	0.1794	0.1393	0.3207	0.7785	0.0222	0.0310	0.2121

Table 3: Components of the error indicator for each refinement step for the cantilever, the bridge, and the L-shaped domain.

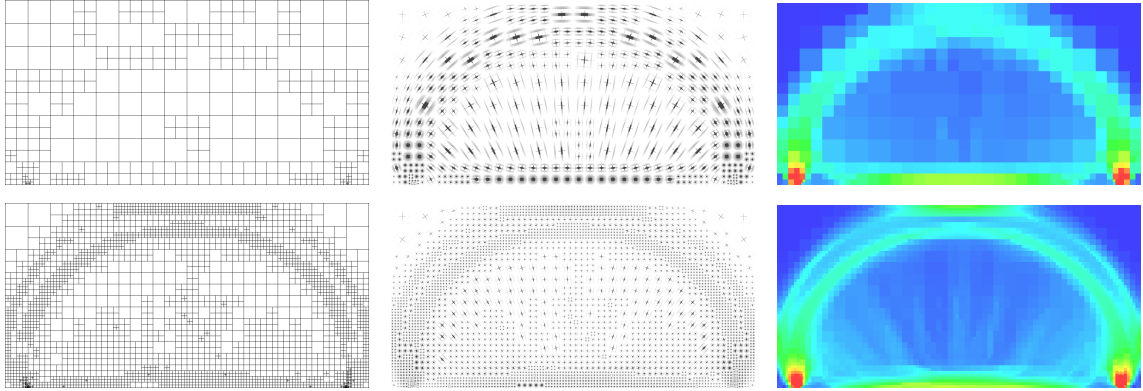


Figure 6: For the bridge scenario after 4 / 9 refinement steps: adaptively refined grid; visualization of the two-scale model as in Figure 3; von Mises stress with color coding as in Figure 3 for values in $[0, 8]$.

the grid scale and should be considered as an indication of the limits of the approximate microscopic model used in the algorithm. The proposed error indicators robustly reports this turning point where the algorithm could be stopped. Hence, the proposed algorithm allows to identify an adaptive mesh on which the physical realization of a close to optimal microstructure is mechanically easier

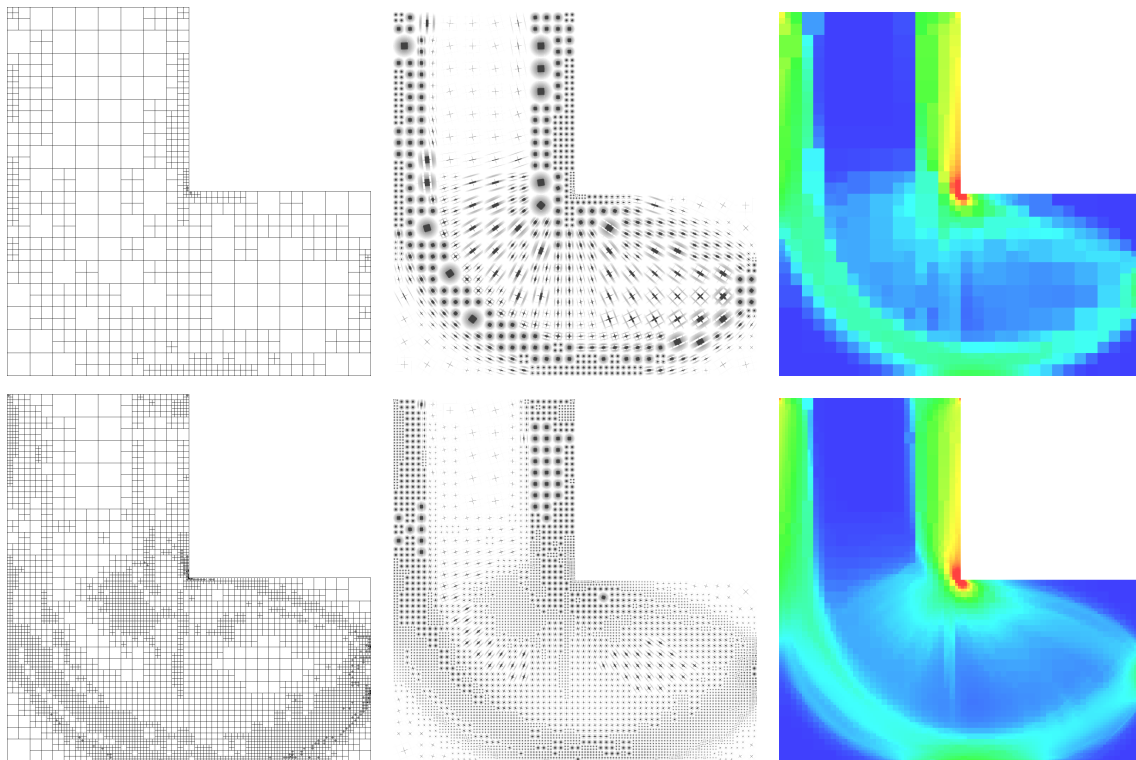


Figure 7: For the L-shaped domain after 4 / 9 refinement steps: adaptively refined grid; visualization of the two-scale model as in Figure 3; von Mises stress with color coding as in Figure 3 for values in $[0, 4]$.

and possibly more realistic, and helps to avoid overrefinement.

Acknowledgments

This work has been supported by the *Deutsche Forschungsgemeinschaft* through *Collaborative Research Centre 1060 – The Mathematics of Emergent Effects*.

References

- [1] G. Allaire, E. Bonnetier, G. Francfort, and F. Jouve. Shape optimization by the homogenization method. *Numerische Mathematik*, 76:27–68, 1997.
- [2] G. Allaire and R. V. Kohn. Optimal design for minimum weight and compliance in plane stress using extremal microstructures. *European J. Mech. A Solids*, 12(6):839–878, 1993.
- [3] G. Allaire. *Shape optimization by the homogenization method*, volume 146 of *Applied Mathematical Sciences*. Springer-Verlag, New York, 2002.
- [4] G. Allaire and R. V. Kohn. Explicit optimal bounds on the elastic energy of a two-phase composite in two space dimensions. *Quart. Appl. Math.*, 51(4):675–699, 1993.
- [5] P. Atwal, S. Conti, B. Geihe, M. Pach, M. Rumpf, and R. Schultz. On shape optimization with stochastic loadings. In G. Leugering, S. Engell, A. Griewank, M. Hinze, R. Rannacher, V. Schulz, M. Ulbrich, and S. Ulbrich, editors, *Constrained Optimization and Optimal Control for Partial Differential Equations*, volume 160 of *International Series of Numerical Mathematics*, chapter 2, pages 215–243. Springer, Basel, 2012.

- [6] M. Avellaneda. Optimal bounds and microgeometries for elastic two-phase composites. *SIAM J. Appl. Math.*, 47(6):1216–1228, 1987.
- [7] C. Barbarosie and A.-M. Toader. Shape and topology optimization for periodic problems. I. The shape and the topological derivative. *Struct. Multidiscip. Optim.*, 40(1-6):381–391, 2010.
- [8] C. Barbarosie and A.-M. Toader. Shape and topology optimization for periodic problems. II. Optimization algorithm and numerical examples. *Struct. Multidiscip. Optim.*, 40(1-6):393–408, 2010.
- [9] C. Barbarosie and A.-M. Toader. Optimization of bodies with locally periodic microstructure. *Mechanics of Advanced Materials and Structures*, 19(4):290–301, 2012.
- [10] R. Becker, E. Estecahandy, and D. Trujillo. Weighted marking for goal-oriented adaptive finite element methods. *SIAM Journal on Numerical Analysis*, 49(6):2451–2469, 2011.
- [11] R. Becker, H. Kapp, and R. Rannacher. Adaptive finite element methods for optimal control of partial differential equations: Basic concept. *SIAM J. Control Optim.*, 39(1):113–132, 2000.
- [12] R. Becker and R. Rannacher. A feed-back approach to error control in finite element methods: Basic analysis and examples. *Computational Mechanics*, 5:434–446, 1997.
- [13] M. P. Bendsøe. *Optimization of structural topology, shape, and material*. Springer-Verlag, Berlin, 1995.
- [14] O. Benedix and B. Vexler. A posteriori error estimation and adaptivity for elliptic optimal control problems with state constraints. *Computational Optimization and Applications*, 44:3–25, 2009.
- [15] A. Braides and A. Defranceschi. *Homogenization of Multiple Integrals*. Claredon Press, Oxford, 1998.
- [16] C. Brandenburg, F. Lindemann, M. Ulbrich, and S. Ulbrich. Advanced numerical methods for pde constrained optimization with application to optimal design in navier stokes flow. In G. Leugering, S. Engell, A. Griewank, M. Hinze, R. Rannacher, V. Schulz, M. Ulbrich, and S. Ulbrich, editors, *Constrained Optimization and Optimal Control for Partial Differential Equations*, volume 160 of *International Series of Numerical Mathematics*, pages 257–275. Springer Basel, 2012.
- [17] G. Buttazzo and G. Dal Maso. Shape optimization for dirichlet problems: Relaxed formulation and optimality conditions. *Applied Mathematics and Optimization*, 23:17–49, 1991.
- [18] A. Cherkasov. *Variational methods for structural optimization*, volume 140 of *Applied Mathematical Sciences*. Springer-Verlag, New York, 2000.
- [19] P. G. Ciarlet. *The finite element method for elliptic problems*. North-Holland Publishing Company, 1978.
- [20] D. Cioranescu and P. Donato. *An Introduction to Homogenization*. Oxford University Press, Oxford, 1999.
- [21] S. Conti, B. Geihe, M. Rumpf, and R. Schultz. Two-stage stochastic optimization meets two-scale simulation. In G. Leugering, P. Benner, S. Engell, A. Griewank, H. Harbrecht, M. Hinze, R. Rannacher, and S. Ulbrich, editors, *Trends in PDE Constrained Optimization*, volume 165 of *International Series of Numerical Mathematics*, pages 193–211. Springer International Publishing, 2014.
- [22] M. C. Delfour and J. Zolésio. *Geometries and Shapes: Analysis, Differential Calculus and Optimization*. Adv. Des. Control 4. SIAM, Philadelphia, 2001.
- [23] W. Dörfler. A convergent adaptive algorithm for Poisson’s equation. *SIAM J. Numer. Anal.*, 33(3):1106–1124, June 1996.

- [24] W. E and B. Engquist. The heterogeneous multiscale methods. *Commun. Math. Sci.*, 1(1):87–132, 2003.
- [25] W. E and B. Engquist. The heterogeneous multi-scale method for homogenization problems. In *Multiscale Methods in Science and Engineering*, volume 44 of *Lecture Notes in Computational Science and Engineering*, pages 89–110. Springer Berlin Heidelberg, 2005.
- [26] W. E, B. Engquist, and Z. Huang. Heterogeneous multiscale method: A general methodology for multiscale modeling. *Physical Review B*, 67(9):092101–1–092101–4, March 2003.
- [27] W. E, P. Ming, and P. Zhang. Analysis of the heterogeneous multiscale method for elliptic homogenization problems. *J. Amer. Math. Soc.*, 18(1):121–156, 2005.
- [28] G. A. Francfort and F. Murat. Homogenization and optimal bounds in linear elasticity. *Arch. Rational Mech. Anal.*, 94(4):307–334, 1986.
- [29] B. Geihe and M. Rumpf. A posteriori error estimates for sequential laminates in shape optimization. In *DCDS-S Special issue on Homogenization-Based Numerical Methods*. 2015. to appear.
- [30] L. Gibiansky and A. Cherkaev. Microstructures of composites of extremal rigidity and exact estimates of the associated energy density. *Ioffe Physicotechnical Institute*, 1115, 1987.
- [31] Y. Grabovsky and R. V. Kohn. Microstructures minimizing the energy of a two phase elastic composite in two space dimensions. I. The confocal ellipse construction. *J. Mech. Phys. Solids*, 43(6):933–947, 1995.
- [32] Z. Hashin. The elastic moduli of heterogeneous materials. *Trans. ASME Ser. E. J. Appl. Mech.*, 29:143–150, 1962.
- [33] J. Haslinger, M. Kočvara, G. Leugering, and M. Stingl. Multidisciplinary free material optimization. *SIAM Journal on Applied Mathematics*, 70(7):2709–2728, 2010.
- [34] P. Henning and M. Ohlberger. The heterogeneous multiscale finite element method for elliptic homogenization problems in perforated domains. *Numerische Mathematik*, 113, Issue 4:601–629, october 2009.
- [35] V. V. Jikov, S. M. Kozlov, and O. A. Oleĭnik. *Homogenization of differential operators and integral functionals*. Springer-Verlag, Berlin, 1994.
- [36] F. Jouve and E. Bonnetier. Checkerboard instabilities in topological shape optimization algorithms. In *Proceedings of the Conference on Inverse Problems, Control and Shape Optimization (PICO’98), Carthage (1998)*, 1998.
- [37] L. Kaland, J. C. De Los Reyes, and N. R. Gauger. One-shot methods in function space for pde-constrained optimal control problems. *Optimization Methods and Software*, 29(2):376–405, 2014.
- [38] L. Kaland. *The one-shot method : function space analysis and algorithmic extension by adaptivity*. Dissertation, RWTH Aachen, 2013.
- [39] B. Kiniger and B. Vexler. A priori error estimates for finite element discretizations of a shape optimization problem. *ESAIM: Mathematical Modelling and Numerical Analysis*, 47:1733–1763, 11 2013.
- [40] P. Kogut and G. Leugering. Matrix-Valued L^1 -Optimal Controls in the Coefficients of Linear Elliptic Problems. *Z. Anal. Anwend.*, 32(4):433–456, 2013.
- [41] R. V. Kohn and R. Lipton. Optimal bounds for the effective energy of a mixture of isotropic, incompressible, elastic materials. *Arch. Rational Mech. Anal.*, 102(4):331–350, 1988.

- [42] D. Leykekhman, D. Meidner, and B. Vexler. Optimal error estimates for finite element discretization of elliptic optimal control problems with finitely many pointwise state constraints. *Computational Optimization and Applications*, 55(3):769–802, 2013.
- [43] K. A. Lurie and A. V. Cherkaev. Effective characteristics of composite materials and the optimal design of structural elements. *Adv. in Mech.*, 9(2):3–81, 1986.
- [44] G. W. Milton. *The Theory of Composites*. Cambridge University Press, 2002.
- [45] P. Morin, R. Nochetto, M. Pauletti, and M. Verani. Adaptive sqp method for shape optimization. In G. Kreiss, P. Lötstedt, A. Målqvist, and M. Neytcheva, editors, *Numerical Mathematics and Advanced Applications 2009*, pages 663–673. Springer Berlin Heidelberg, 2010.
- [46] P. Morin, R. H. Nochetto, M. S. Pauletti, and M. Verani. Adaptive finite element method for shape optimization. *ESAIM: Control, Optimisation and Calculus of Variations*, 18:1122–1149, 10 2012.
- [47] F. Murat and L. Tartar. Calcul des variations et homogénéisation. In *Homogenization methods: theory and applications in physics (Bréau-sans-Nappe, 1983)*, volume 57 of *Collect. Dir. Études Rech. Élec. France*, pages 319–369. Eyrolles, Paris, 1985.
- [48] J. T. Oden and K. Vemaganti. Adaptive modeling of composite structures: Modeling error estimation. *International Journal for Computational Civil and Structural Engineering*, 1:1–16, 2000.
- [49] J. T. Oden and K. S. Vemaganti. Estimation of local modeling error and goal-oriented adaptive modeling of heterogeneous materials. I. Error estimates and adaptive algorithms. *J. Comput. Phys.*, 164(1):22–47, 2000.
- [50] M. Ohlberger. A posteriori error estimates for the heterogeneous multiscale finite element method for elliptic homogenization problems. *SIAM Multiscale Mod. Simul.*, 4(1):88–114, 2005.
- [51] S. Prudhomme and J. T. Oden. On goal-oriented error estimation for elliptic problems: application to the control of pointwise errors. *Comput. Methods Appl. Mech. Engrg.*, 176(1-4):313–331, 1999. New advances in computational methods (Cachan, 1997).
- [52] O. Steinbach. *Numerische Näherungsverfahren für elliptische Randwertprobleme: Finite Elemente und Randelemente*. B. G. Teubner, Wiesbaden, 2003.
- [53] L. Tartar. Estimations fines des coefficients homogénéisés. In *Ennio De Giorgi colloquium (Paris, 1983)*, volume 125 of *Res. Notes in Math.*, pages 168–187. Pitman, Boston, MA, 1985.
- [54] K. Vemaganti. Modelling error estimation and adaptive modelling of perforated materials. *Internat. J. Numer. Methods Engrg.*, 59(12):1587–1604, 2004.
- [55] B. Vexler and W. Wollner. Adaptive finite elements for elliptic optimization problems with control constraints. *SIAM Journal on Control and Optimization*, 47(1):509–534, 2008.
- [56] S. Vigdergauz. Two-dimensional grained composites of extreme rigidity. *Journal of Applied Mechanics*, 61(2):390–394, 1994.
- [57] A. Wächter. *An Interior Point Algorithm for Large-Scale Nonlinear Optimization with Applications in Process Engineering*. Phd thesis, Carnegie Mellon University, 2002.
- [58] A. Wächter and L. Biegler. On the implementation of a primal-dual interior point filter line search algorithm for large-scale nonlinear programming. *Mathematical Programming*, 106(1):25–57, 2006.
- [59] W. Wollner. Goal-oriented adaptivity for optimization of elliptic systems subject to pointwise inequality constraints: Application to free material optimization. *PAMM*, 10(1):669–672, 2010.